BL-16A/2015G690

Structural and Magnetic properties of non-stoichiometric Mn-poor $LaSrMnO_3$

Hiroshi Naganuma [1, 2*]

[1] Graduate School of Engineering, Tohoku University, Sendai 980-8579, Japan

[2] Unité Mixte de Physique, CNRS, Thales, 91767 Palaiseau, France

1 Introduction

Perovskite $LaSrMnO_3$ (LSMO) with a rhombohedral crystal symmetry has a high carrier spin polarization. Here, it is of interest in spintronics devices as a spin source. (1) The phase diagram for LSMOs with various La and Sr compositions shows the presence of not only rhombohedral but also a variety of other crystal symmetries. Moreover, the electric and magnetic properties of LSMO depend on its crystal symmetry. (2 - 9) The highest Curie temperature (T_C) above room temperature (RT) with metallic conductivity is obtained for $La_{0.6}Sr_{0.4}Mn_{1.0}O_3$ processing a rhombohedral crystal symmetry. Therefore, adjusting the composition to achieve a rhombohedral structure is important in LSMO materials. (9) The previous reports mainly focused on the La/Sr composition dependence while fixing the Mn composition at 1.0. And also, the oxygen vacancy strongly influences on the structural, electric and magnetic properties. The X-ray absorption spectroscopy (XAS) is the one of the strong tool for estimating the oxygen vacancy. In this study, Mn-poor LSMO films were prepared on $SrTiO_3$ (STO) (100) substrates by reactive radio frequency (RF) magnetron sputtering, and the effect of annealing temperature in air on their structure, magnetic properties was investigated by multi-prove analysis.

2 Experimental procedure

LSMO films (50 nm) were grown on the STO (100) substrates by reactive RF magnetron sputtering (ULVAC Techno. Ltd). The sputtering chamber was evacuated to below 2×10^{-6} Pa. A $La_{0.6}Sr_{0.4}Mn_{1.0}O_x$ sintered target of 2 inches in diameter was used. The sputtering power and substrate temperature (T_s) during sputtering were fixed at 100 W and 650°C, respectively. The total pressure (P_{Ar+O2}) of the Ar + O_2 gaseous mixture was fixed at P_{Ar+O2} = 0.4 Pa, where P_{O2} was 5%. These samples were annealed in air at temperatures between 650 and 950°C for 2 hours. In the case of sputtering deposition method, the film composition becomes different from composition of sputtering target due to different in sputtering rate in each element. The composition of samples was multifaceted checked by inductively coupled plasma atomic emission spectroscopy (ICP-AES: SPS-4000, SII). The ICP-AES analysis revealed that the film composition was $La_{0.55}Sr_{0.08}Mn_{0.37}O_3$ which indicates a Mn-poor composition. There is no experimental report on the structural and magnetic properties of LSMO at this composition. The perovskite LSMO is complicated to assign the crystal symmetry because the crystal symmetry continuously changed by composition ratio. Crystal structure was multilaterally evaluated by XRD (Discover D8 equipped with 2D detector, Bulker Co Ltd) analysis and the EBSD attached to the SEM. The LSMO is complicated in magnetic properties because the its changed by not only composition ratio by also oxygen vacancy. The XAS and X-ray magnetic circular dichroism (XMCD) measurements was carried out to determine electric and magnetic properties of LMSO films. XMCD measurement was done at RT at the Mn $L_{2,3}$ absorption edges. XAS were obtained by total electron yield (TEY) method. The background was simply subtracted by liner fitting. The circularly polarized APPLE type undulators were used. (10) The degree of circular polarization (P_c) was $P_c \sim 1$. The magnetic field of 10 kOe was applied to 55 degrees off normal from the film plane. Magnetization (M - H) curves and temperature dependence of magnetization (M - T) was measured using a superconducting quantum interference device (SQUID) magnetometer.

3 Results and discussion

A: SQUID and VSM measurements

The T_C of $La_{0.7}Sr_{0.3}Mn_{1.0}O_3$ increases by post-annealing in air due to the effect of oxygen supply and the promotion of crystallization. (11, 12) The Mn-poor LSMO films were annealed in air at various temperatures (T_a). Figure 1(a) shows the annealing temperature (T_a) dependence of magnetization of the Mn-poor LSMO films (50 nm) i.e., the M - H curves measured at RT. Figure 1(b) shows the M - T curves for the Mn-poor LSMO films. The M – H curves showed low remanence, and the saturation magnetization (M_s) increased by increasing the T_a. The T_C increased at T_a = 650ºC, which is as same temperature as T_s of 650ºC of the as-made sample. The difference between the T_s and T_a lies in whether the heating was done in vacuum or in air. This indicate that annealing in air effectively supplies oxygen to the perovskite structure of the Mn-poor LSMO films. The T_C of the Mn-poor LSMO films increased with increasing T_a and became T_C higher than RT at $T_a \geq$ 861°C. This tendency of the T_C is in agreement with the increase in the M_s by an increase in the T_a.

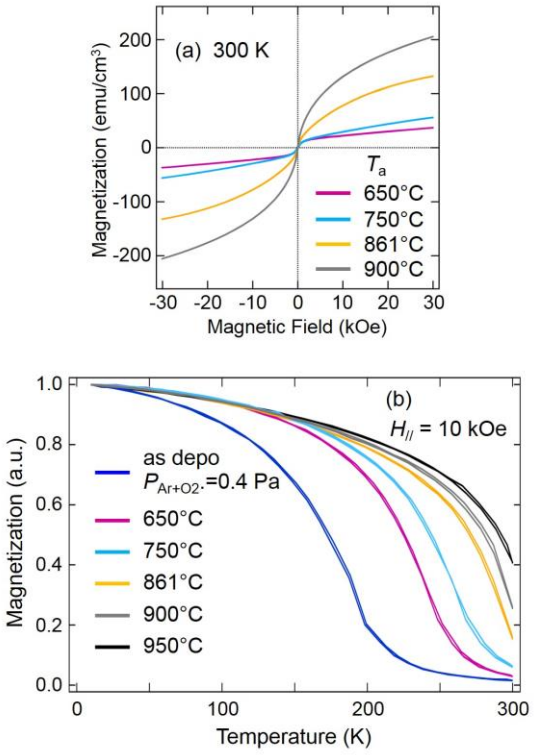

Fig. 1(a) Magnetization (*M* - *H*) curves of LSMO with various annealing temperatures (T_a), (b) temperature dependence of magnetization (*M* - *T*) for the samples annealed in air at various temperatures (T_a). Samples grown at P_{Ar}+O_2 = 0.4 Pa were the ones annealed.

B: XAS and XMCD measurements

In order to investigate the electric and magnetic properties of Mn in the LSMO, XAS and XMCD measurements were carried out. Figure 2(a) shows the XAS, and 2(b) XMCD spectra of the Mn $L_{2,3}$ edges, and 2(c) element-specific hysteresis loops at 643 eV for the LSMO film (70 nm) grown epitaxially on the STO substrate at T_a = 861°C. In Fig. 2(a), the XAS spectra for the opposite directions of the external magnetic field are denoted as μ_+ and μ_-, respectively. The XAS spectra were applied at an inclination of 55° to the nominal direction because at this inclination, the noise caused by the reversed electron during the TEY method is reduced. The XAS peak was clearly split into 641 and 643 eV, and the peak at 641 eV was relatively stronger than that obtained for the stoichiometric $La_{0.7}Sr_{0.3}MnO_3$ films. (13, 14) The reasons for the increase in the intensity of the peak observed at 641 eV are the oxygen vacancy (formation of divalent Mn), (15, 16) epitaxial strain, (17) and dimensional effect. (17) The thickness of the LSMO film was found to be 70 nm, and the epitaxial strain and dimensional effect could be excluded for the surface sensitive XAS measurement. Although the sample was post-annealed in air, it can be concluded that the oxygen vacancy still remained and a divalent Mn was formed. The XMCD spectrum was obtained by the subtraction of μ_+ from μ_-. [Fig. 2(b)] The elemental specific hysteresis loops were measured at 643 eV where showed relatively large XMCD intensity. [Fig. 2(c)] The influence of the reversed electron can not be neglected near zero magnetic field; the noise level was large. The elemental specific hysteresis loop clearly shows that the sign of the XMCD changed with a change in the direction of the external magnetic field. The XMCD spectrum of LSMO films obtained here was consistent with that obtained in previous studies. (16, 17) These XAS and XMCD measurement address the electric state of oxygen and it seems the oxygen vacancy was existed in LSMO films. The magnetic moment of Mn is also similar to the *M* – *H* curve measured by SQUID indicates the total magnetic response as a function of external field is represented by Mn moment. These kinds of important information can be obtained only by using the elemental specific XMCD technique.

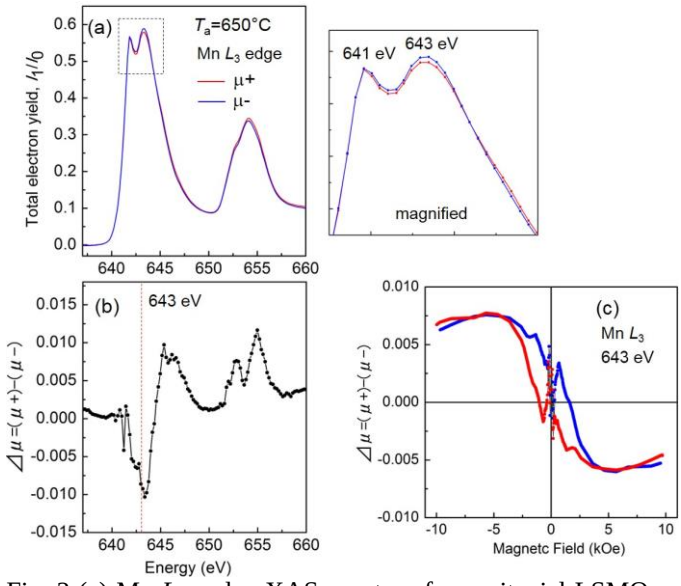

Fig. 2 (a) Mn $L_{2,3}$ edge XAS spectra of an epitaxial LSMO film on STO substrate, right (μ_+) and left (μ_-) handed circularly polarization, (b) XMCD spectrum μ_+ - μ_-. (c) elemental-specific hysteresis loops at 643 eV. External magnetic field was applied at 55-degrees off-normal from the film plane.

C: XRD measurements

Figure 3(a) shows the 2 theta - chi maps for the samples annealed at T_a = 650°C, 3(b) 2-theta-scan profiles at chi = 0°, and 3(c) schematic illustration of epitaxial relation of the LSMO on STO substrate. At chi = 90°, XRD spots corresponding to the (111), (212), and (313) were observed along the 2 theta direction. These spots correspond to the monoclinic / orthorhombic structure; and almost disappeared in the 2 theta-chi XRD maps at annealing temperatures higher than 650°C. From the 2 theta profiles at chi = 0°, it can be seen clearly that the weak XRD peaks were located at higher angles associated with STO, which is usually identified as a (036) rhombohedral structure of LSMO. (18) The number of XRD peaks were small when compared with the bulk rhombohedral LSMO because of the epitaxial growth and the lack of oxygen vacancies. A shift in the XRD peaks to

lower values can be attributed to oxygen vacancy in the rhombohedral structure of LSMO. (19, 20) This existence of oxygen vacancy is consistent with the XAS result. It can be seen from the XRD patterns that the STO and rhombohedral LSMO peaks are located close to each other, making it difficult to distinguish between the two.

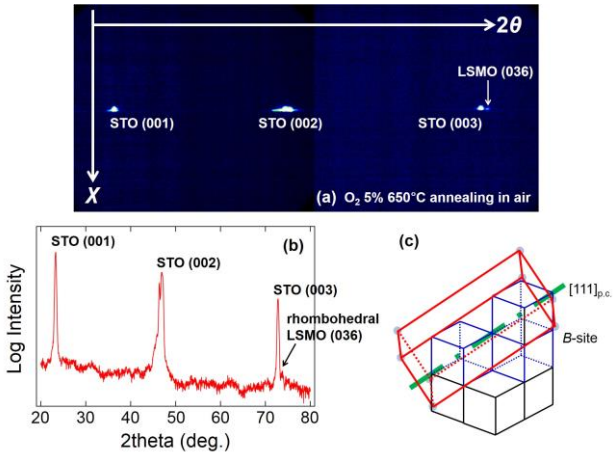

Fig. 3 (a) 2 theta-chi XRD maps (b) 2-theta scan profiles at chi = 0° for the samples annealed in air at 861°C for 2 hours. (c) Schematic illustration of epitaxial relation of the rhombohedral LSMO on STO substrate.

D: EBSD measurements

In order to confirmed the multilateral crystal symmetry after the annealing, the inelastic scattering method of EBSD was used. EBSD is an effective analytical method for the determination of crystal symmetry of complex oxide materials. (21, 22) The diffraction depth of EBSD is a few nanometers owing to which it excludes information on the crystal structure of the substrate. As mentioned in the XRD part, the rhombohedral LSMO has a crystal symmetry similar to that of the STO substrate; therefore, exclusive information on the crystal structure of the STO substrate can be an accurate evaluation of the crystal structure of LSMO. The EBSD method is useful to determine the crystal symmetry of the LSMO films having a variety of crystal symmetries, which change continuously with composition. Electron diffraction was carried out over a wide area on the surface of the film. Figure 4(a) shows the EBSD image and 4(b) fitting result using a rhombohedral symmetry for the sample annealed at 920°C for 2 h. We also tried to fit the EBSD patterns to tetragonal and monoclinic crystal symmetry; however, the EBSD patterns could not be fit. The EBSD profile of the non-stoichiometric Mn-poor LSMO film was almost perfectly identified by a rhombohedral structure as shown in Fig. 4(b). From the EBSD results, it can be considered that the XAS peak at 641 eV was not appeared by the segregation and formation of MnO during the annealing process. (23) Because the EBSD patterns did not show any evidence of the cubic pattern. MnO is not a magnetic material; therefore, the XMCD results also support these derived relations. Hence, it can be concluded that the relatively large intensity of the XAS peak at 641 eV was due to the oxygen vacancy in the non-stoichiometric Mn-poor LSMO film having a rhombohedral crystal symmetry. The XRD profiles to out-of-plane also included the information of the STO substrate; therefore, it becomes complicated as shown in Fig. 3. EBSD could exclude the information from substrate and then it showed clear differences among these complexes perovskite structures. Upon heat treatment in the air, the T_C of the stoichiometric $La_{0.7}Sr_{0.3}Mn_{1.0}O_3$ increases. It should be noted that the Mn-poor non-stoichiometric LSMO films could exhibit almost as same characterization such as high T_c and metallic conductivity when the samples were annealed in air. Furthermore, a systematic investigation of the Mn composition dependence of LSMO on XAS is necessary in order to understand the relationship between the oxygen vacancy and the magnetic property.

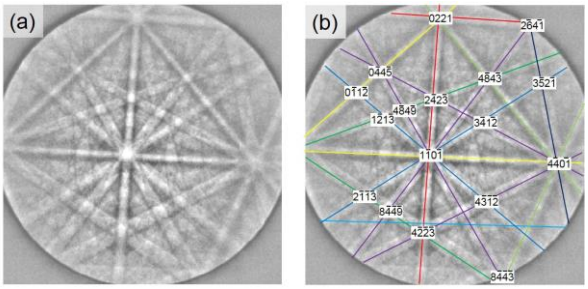

Fig. 4 (a) Electron-backscatter diffraction (EBSD) image for the LSMO annealed at 961°C for 2 hours (b) and EBSD image fitted by rhombohedral crystal symmetry (SG: R3c).

4 Summary

LSMO films were epitaxially grown on the STO (100) substrates by RF magnetron sputtering. The samples were then annealed in air at temperatures in the range of 650 - 950°C. The composition of the Mn-poor LSMO films was determined by ICP-AEP analysis. The 2-theta/chi XRD and EBSD analyses confirmed that the crystal symmetry of the Mn-poor LSMO films was rhombohedral structure. For the samples annealed in air, the T_C increased with increasing T_a, and reached a value higher than RT at $T_a \geq$ 861°C. The transition of the crystal symmetry of the Mn-poor LSMO films affects the magnetic transition. It is expected that the Mn-poor rhombohedral LSMO with a T_C above RT can find application as a high spin-polarized electrode. Finally, it should be noted that these multi-prove analysis effectively understand the materials science; especially, elemental specific measurement has important role in this study.

Acknowledgements

This study was supported by grant-in-aid for scientific research (B) (No. 15H03548), grant-in-aid for scientific research (S) (No. 24226001), and the Leading Young Researcher Overseas Visit Program. XAS and XMCD measurement was carried out at BL-16A, at the Photon Factory in Institute of Materials Structure Science, High

Energy Accelerator Research Organization, Japan (proposal number: 2015G690)

References

[1] S. Majumdar and S. Dijken, Pulsed laser deposition of $La_{1-x}Sr_xMnO_3$: thin-film properties and spintronic applications, J. Phys. D: Appl. Phys. **47** (2014) 034010.

[2] J. -L. Maurice, R. Lyonnet, J. -P. Contour, Transmission electron microscopy of $La_{0.67}Sr_{0.33}MnO_3/SrTiO_3/La_{0.67}Sr_{0.33}MnO_3$ heterostructures grown by pulsed laser deposition on (001) $SrTiO_3$, J. Mag. Mag. Mat., **211** (2000) 91.

[3] Li, Tingxian; Li, Kuoshe; Hu, Zhou, Thickness and frequency dependence of magnetoelectric effect for epitaxial $La_{0.7}Sr_{0.3}MnO_3/BaTiO_3$ bilayer, J. Alloy Comp., **592** (2014) 266.

[4] R. Nori, S. N. Kale, U. Ganguly, N. R. C. Raju, D. S. Sutar, R. Pinto and V. R. Rao, Morphology and Curie temperature engineering in crystalline $La_{0.7}Sr_{0.3}MnO_3$ films on Si by pulsed laser deposition, J. Appl. Phys. **115** (2014) 033518.

[5] Y. P. Lee, S. Y. Park, Y. H. Hyun, J. B. Kim, V. G. Prokhorov, V. A. Komashko, and V. L. Svetchnikov, Microstructural and magnetotransport properties of $La_{0.7}Ca_{0.3}MnO_3/BaTiO_3$ and $La_{0.7}Sr_{0.3}MnO_3/BaTiO_3$ bilayered films, Phys. Rev. B, **73** (2006) 224413.

[6] T. Namikawa, K. Kaneta, N. Matsushita, S. Nakagawa, M. Naoe, Annealing Effect of Magnetic Characteristics of (La,Sr)MnO_3 Sputtered Films, IEEE Trans. Magn. Mat., **35** (1999) 2850.

[7] Z. Yang, L. Sun, C. Ke, X. Chen, W. Zhu, and O. Tan, Growth and structure properties of $La_{1-x}Sr_xMnO_{3-\sigma}$ (x = 0.2, 0.3, 0.45) thin film grown on $SrTiO_3$ (001) single-crystal substrate by laser molecular beam epitaxy, J. Crys. Grow. **311** (2009) 3289.

[8] A. Dagotto, T. Hotta and A. Moreo, Colossal Magnetoresistant Materials: The Key Role of Phase Separation, Phys. Rep. **344** (2001) 1.

[9] J. Hemberger, A. Krimmel, T. Kurz, H. -A. Krug von Nidda, V. Y. Ivanov, A. A. Mukhin, A. M. Balbashov, and A. Loidl, Structural, magnetic, and electrical properties of single-crystalline $La_{1-x}Sr_xMnO_3$ ($0.4 < x < 0.85$), Phys. Rev. B, **66** (2002) 094410.

[10] Amemiya, K.; Toyoshima, A.; Kikuchi, T.; Kosuge, T.; Nigorikawa, K.; Sumii, R.; and Ito, K. Commissioning of a Soft X‐ray Beamline PF‐BL‐16A with a Variable‐Included‐Angle Varied‐Line‐Spacing Grating Monochromator, AIP Conf. Proc. **1234** (2010) 295.

[11] T. Li, B. Wang, H. Dai, Y. Du, H. Yan, and Y. Liu, Annealing effect on the structural and magnetic properties of $La_{0.7}Sr_{0.3}MnO_3$ films, J. Appl. Phys. **98** (2005) 123505.

[12] D. R. Sahu, D. K. Mishra, J.-L. Huang, B. K. Roul, Annealing effect on the properties of $La_{0.7}Sr_{0.3}MnO_3$ thin film grown on Si substrates by DC sputtering, Physica B, **396** (2007) 75.

[13] S. Stadler, Y. U. Idzerda, Z. Chen, S. B. Ogale, and T. Venkatesan, The magnetism of a buried $La_{0.7}Sr_{0.3}MnO_3$ interface, Appl. Phys. Lett. **75** (1999) 3384.

[14] J.-H. Park, E. Vescovo, H.-J. Kim, C. Kwon, R. Ramesh, and T. Venkatesan, Magnetic Properties at Surface Boundary of a Half-Metallic Ferromagnet $La_{0.7}Sr_{0.3}MnO_3$, Phys. Rev. Lett., **81** (1998) 1953.

[15] M. Bowen, M. Bibes, A. Barthélémy, J.-P. Contour, A. Anane, Y. Lemaître, and A. Fert, Nearly total spin polarization in $La_{2/3}Sr_{1/3}MnO_3$ from tunneling experiments, Appl. Phys. Lett. **82** (2003) 233.

[16] M. P. de Jong, I. Bergenti, V. A. Dediu, M. Fahlman, M. Marsi, and C. Taliani, Evidence for Mn^{2+} ions at surfaces of $La_{0.7}Sr_{0.3}MnO_3$ thin films, Phys. Rev. B, **71** (2005) 014434.

[17] J.-S. Lee, D. A. Arena, P. Yu, C. S. Nelson, R. Fan, C. J. Kinane, S. Langridge, M. D. Rossell, R. Ramesh, and C. -C. Kao, Hidden Magnetic Configuration in Epitaxial $La_{1-x}Sr_xMnO_3$ Films, Phys. Rev. Lett., **105** (2010) 257204.

[18] D. Schumacher, A. Steffen, J. Voigt, J. Schubert, and T. Brückel, Inducing exchange bias in La $0_{.67}Sr0_{.33}MnO_{3-\delta}/SrTiO_3$ thin films by strain and oxygen deficiency, Phys. Rev. B, **88** (2013) 144427.

[19] J. Li, J. -M. Liu, H. P. Li, H. C. Fang, C. K. Ong, Magnetoresistance in oxygen deficient $La_{0.75}Sr_{0.25}MnO_{3\sim d}$ thin films prepared by pulsed laser deposition, J. Mag. Mag. Mat., **202** (1999) 285.

[20] D. Schumacher, A. Steffen, J. Voigt, J. Schubert, and Th. Brückel, Inducing exchange bias in $La_{0.67}Sr_{0.33}MnO_{3-\delta}/SrTiO_3$ thin films by strain and oxygen deficiency, Phys. Rev. B, **88** (2013) 144427.

[21] Y. Zhang, A. M. Schultz, L. Li, H. Chien, P. A. Salvador, G. S. Rohrer, Combinatorial substrate epitaxy: A high-throughput method for determining phase and orientation relationships and its application to $BiFeO_3/TiO_2$ heterostructures, Acta Meterialia, **60** (2012) 6486.

[22] D. Pravarthana, M. Trassin, Jiun Haw Chu, M. Lacotte, A. David, R. Ramesh, P. A. Salvador, and W. Prellier, $BiFeO_3/La_{0.7}Sr_{0.3}MnO_3$ heterostructures deposited on spark plasma sintered $LaAlO_3$ substrates Appl. Phys. Lett., **104** (2014) 082914.

[23] C. Mitra, Z. Hu, P. Raychaudhuri, S. Wirth, S. I. Csiszar, H. H. Hsieh, H. -J. Lin, C. T. Chen, and L. H. Tjeng, Direct observation of electron doping in $La_{0.7}Ce_{0.3}MnO_3$ using x-ray absorption spectroscopy, Phys. Rev. B, **67** (2003) 092404.

* naganumahiroshi1@gmail.com